Unconventional orientational glass transitions in symmetrical difluorotetrachloroethane

1994 J. Phys.: Condens. Matter 6 6947

(http://iopscience.iop.org/0953-8984/6/35/006)

J. Phys.: Condens. Matter 6 (1994) 6947–6964. Printed in the UK

Unconventional orientational glass transitions in symmetrical difluorotetrachloroethane

J K Krüger†, J Schreiber†‖, R Jiménez†, K-P Bohn†, F Smutný‡, M Kubát‡, J Petzelt‡, J Hrabovská-Bradshaw‡, S Kamba‡ and J F Legrand§

† Fachrichtung Experimentalphysik 10.2, Universität des Saarlandes, Bau 38, Postfach 151150, D-66041 Saarbrücken, Germany

‡ Institute of Physics, Academy of Sciences of the Czech Republic, Na Solvance 2, 18040 Praha 8 - Libeň, Czech Republic

§ Laboratoire de Spectrométrie Physique, BP 87, Université de Grenoble, 38402 Saint Martin d'Hères Cédex, France

Received 21 January 1994, in final form 14 April 1994

Abstract. Frozen-in *trans* and *gauche* conformational disorder of symmetrical difluorotetrachloroethane (DFTCE) produces the tendency of this plastic crystal to form an orientational glassy state on cooling below $T_g = 86$ K. To throw light upon the freezing mechanism in DFTCE neutron diffraction and Brillouin scattering as well as infrared and dielectric measurements are employed. The overall picture of the results obtained can be characterized in terms of a classical glass-transition process with a relaxation frequency obeying the Vogel–Fulcher law. However, a more sophisticated picture of the freezing process is indicated by a quantitative analysis of the new Brillouin data, e.g. the temperature dependence of the sound velocity. The behaviour could be understood on the basis of a mode-coupling theory.

1. Introduction

The understanding of the nature of glass transitions in canonical and orientational glass formers is an exciting task and has been the subject of numerous experimental and theoretical works (e.g. [1–5]) in the last few years. The search for model substances led to the study of simple compounds that contain predominantly orientational disorder of the constituting molecules. Plastic crystals often represent such kinds of material. While the molecules in liquids are free to displace and rotate, in plastic crystals the molecules have their average centre of gravity fixed at lattice positions but they can rotate almost freely or jump rather fast between different orientations. This dynamical orientational disorder is slowed down with decreasing temperature. Either long-range orientational order is established via a structural phase transition or a so-called orientational glassy state appears by freezing of the molecular orientational disorder [6]. The latter generally happens if the plastic phase is quenched sufficiently fast. Then the resulting frozen crystalline material shows phenomenological properties typical of canonical glasses. Strong sterical hindrances, competing interactions between molecules and more or less quenched disorder built into the plastic crystal can significantly reduce the necessary quenching rate.

Because of their almost spherical habit many ethane-like molecules are good candidates for forming plastic phases. Hexachloroethane (HCE) is an interesting example with a plastic

‖ Permanent address: Fraunhofer-Institute of Non-destructive Testing, Department of Acoustic Methods for Non-destructive Evaluation and Quality Assurance, Krügerstrasse 22, D-01326 Dresden, Germany.

0953-8984/94/356947+18$19.50

high-temperature phase of cubic symmetry and a melting point $T_m = 458$ K [7]. HCE transforms consecutively into a monoclinic state at $T_{c1} = 344.1$ K and into an orthorhombic one at $T_{c2} = 316.6$ K [7, 8]. The substitution of one Cl by one F atom on each C atom of an HCE molecule results in 1,2-difluoro-1,1,2,2-tetrachloroethane ($CFCl_2$–$CFCl_2$ DFTCE). The energetically non-equivalent *trans* and *gauche* conformations (*trans* with a C_{2h} symmetry and *gauche* with a C_2 symmetry) of DFTCE probably yield one of the necessary frustration mechanisms that make this plastic crystal a good glass former [9, 10].

The plastic phase of DFTCE has a BCC lattice with a melting point at $T_m \simeq 299$ K [11, 12]. The plastic and the adjacent fluid phase have been thoroughly studied using different experimental techniques. Quantitative information was obtained on the bond lengths and bond angles within the molecules (electron diffraction [13]), on the dynamics of the molecular hindered rotations (depolarized Rayleigh scattering [14]), on molecular reorientations and disorder (Raman spectroscopy, ultrasonic investigation [12, 15, 16] and NMR [17]) and on more phenomenological properties such as density, vapour pressure and refractive index of the melt [12]. The melting enthalpy and melting entropy were estimated by Kishimoto *et al* [9] and amount to $\Delta H_m = 3.666$ kJ mol^{-1} and $\Delta S_m = 12.3$ J mol^{-1} K^{-1}. The same authors report a lattice constant $a = 0.718$ nm at $T = 288$ K.

The observation of a pronounced glass-like step in the heat capacity $C_p(T)$ of DFTCE at about $T_g = 90$ K [9] was interpreted as a freezing of hindered molecular reorientations, resulting in static random molecular orientations and, hence, suggested the existence of an orientational glass transition in DFTCE. However, the required conservation of the BCC symmetry was not verified. Two further specific heat anomalies found so far in solid DFTCE occur at 60 K and 130 K [9]. These less pronounced anomalies were attributed to a β-process and to a second freezing process (freezing of the *trans–gauche* transformations), respectively. In order to study the tendency of DFTCE to transform into its thermodynamically stable low-temperature crystalline state Kishimoto *et al* [9] have annealed their sample above its quasi-static glass transition at $T_g + 30$ K. After an annealing time of about two months and then heating their sample in a calorimeter they found a C_p-peak at $T_c = 170$ K. This behaviour was attributed to a transition of the crystalline low-temperature phase (still of unknown symmetry) to the plastic phase. From the related transition enthalpy it was estimated that during the long annealing period only about 3 vol.% of their sample had transformed to the low-temperature crystalline phase. This indicates that DFTCE behaves as a nearly ideal glass former.

Only a few other techniques have been used to study the transition behaviour of solid DFTCE. Initial Brillouin-spectroscopic measurements have been reported for polycrystalline material [18] yielding rather preliminary information on its elastic behaviour. Recent Raman and neutron spectroscopic investigations reveal some peculiarities, pointing to a dynamical glass transition in DFTCE, and their interpretation will be reported elsewhere [19].

The aim of this paper is to present and discuss infrared (IR), neutron-powder-diffraction, dielectric and acoustic data measured on symmetrical DFTCE. Special interest has been paid to the dynamic and quasi-static glass-transition regime. It will be shown that at a first sight our results can be interpreted as a classical glass-transition process in terms of a co-operative α- and β-process with a quasi-static transition at T_g. However, the Brillouin data obtained, e.g. the temperature dependence of the sound velocity, indicate a more sophisticated picture of the freezing process, which can probably be understood on the basis of a mode-coupling theory [20, 21].

2. Experimental details

2.1. Sample preparation

DFTCE used in these investigations was purchased from ICN Biomedicals, Inc., K & K Laboratories (catalogue no 201701) and had a nominal purity of 95%. This material has been further purified using a distillation column of the concentric-annular-gap type with 30 theoretical plates. After four consecutive purification runs the sample had a purity of 99.97%, which was tested by gas chromatography [22].

For dielectric and Brillouin investigations it is desirable to have well defined cuts of single crystals. Appropriate large DFTCE single crystals could be grown by sublimation techniques but, unfortunately, because of their plasticity they could not be cut and polished. Therefore, polycrystalline material was used for all experiments. Because of the cubic symmetry of DFTCE this implies no restrictions within the whole temperature regime for properties described by tensors up to rank two (e.g. dielectric constants). In order to obtain well defined information on the elastic properties of the crystalline state, angle- and space-resolving Brillouin spectroscopy [10, 23, 24] had to be performed on monodomains of polycrystalline samples.

2.2. Infrared spectroscopy (IR)

A special small cuvette with poly-4-methyl-pentene (trade name TPX) windows and a 1 mm Teflon spacer was used for IR measurements. The liquid sample was injected into the cuvette and solidified in such a way that the presence of bubbles within the measured aperture of the sample was minimized. The transmission spectra were measured with an IFS 113v Bruker spectrometer, within the transparency range of TPX ($< 700\ cm^{-1}$).

2.3. Neutron diffraction (ND)

In order to determine the crystal symmetry and the lattice parameter $a(T)$ of DFTCE as a function of temperature, elastic neutron-scattering experiments were performed at the high-flux two-axis diffractometer D-20 (ILL, Grenoble) on powder material. The powder was ground in a cold chamber and put in a cylindrical V can of 5 mm diameter and 30 mm height. The high-flux diffractometer operated at a wavelength of $\lambda = 2.4097$ Å. The position-sensitive detector, covering an angle of 12.6°, was scanned between 20 and 120°. The temperature control of the sample was performed with an He cryostat in the temperature range between about 20 and 270 K. Several cooling and heating runs were performed in order to exclude hysteresis effects on the data.

2.4. Brillouin spectroscopy (BS)

As mentioned above, no large crystal cuts were available for our Brillouin-spectroscopic measurements on DFTCE. Further complications arose from the facts that the material sublimates easily near ambient temperature and that the material sticks to the container walls of the supporting cuvette. As a consequence, on decreasing the temperature the material developed cracks because of increasing mechanical constraints. To overcome this problem we introduced thin transparent spacers between the sample and the cuvette walls in order to relieve mechanical stresses. Brillouin measurements were performed on two kinds of sample: (i) cylindrical samples formed by sublimation in a corresponding cuvette and (ii) film-like samples formed by slow cooling from the melt in a PIA (polymer induced alignment)-coated [24, 25] narrow-spaced cuvette. Both kinds of sample were

polycrystalline, whereby the cylindrical sample consisted of large domains of several millimetres lateral dimensions with the crystal co-ordinate system (x_1, x_2, x_3) oriented in a certain but unspecified manner relative to the laboratory frame (x, y, z). In contrast to the Brillouin data of Wang and Satija [18] the sound-velocity data obtained from our cylindrical sample were measured on a single domain but still with an unknown orientation of the phonon wave vector relative to the crystal axes. It should be mentioned that, because of the cubic symmetry, the optical birefringence plays no role for the Brillouin investigations of polycrystalline DFTCE samples. Moreover, for geometrical reasons the cylindrical samples of type (i) could only be investigated with the help of the conventional 90N scattering geometry (figure 1(*a*)) [10, 26, 27]. However, a general disadvantage of the 90N-scattering technique is the necessity of knowing the refractive index of the sample to calculate the sound velocity from the measured sound frequency.

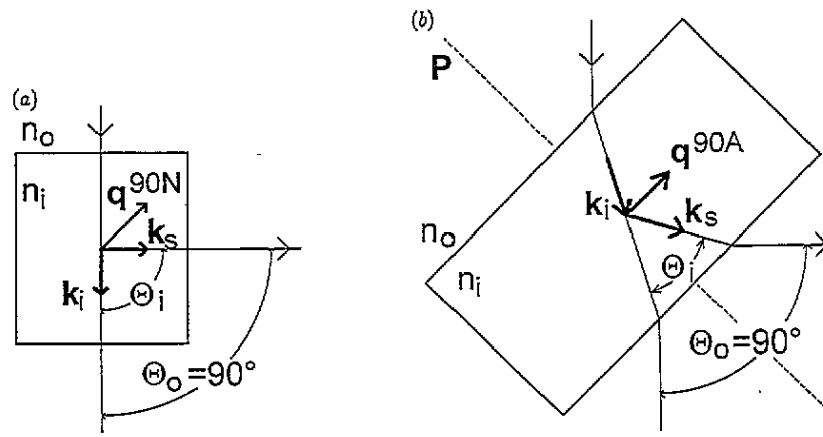

Figure 1. (*a*) Wave vectors of the incident light (k_i) and scattered light (k_s), and the scattering sound-wave vector (q^{90N}) for the 90N scattering geometry. $\Theta_i = 90°$, inner scattering angle; $\Theta_0 = 90°$, outer scattering angle; n_i, refractive index of the sample; n_0, outer refractive index (= 1). (*b*) Wave vectors of the incident light (k_i) and scattered light (k_s), and the scattering sound-wave vector (q^{90A}) for the 90A scattering geometry. Θ_i, inner scattering angle; $\Theta_0 = 90°$, outer scattering angle; n_i, refractive index of the sample; n_0, outer refractive index (= 1); for the 90A scattering geometry Snellius law holds: $n_0 \sin(\Theta_0/2) = n_i \sin(\Theta_i/2)$; *P*, normal to the surface of the plate-like sample.

A technique for the determination of the elastic properties of polycrystalline materials has been presented recently [10, 28] and therefore requires only a short introduction. For elastic solids the velocity $v_\alpha(\hat{q})$ of sound propagation along $\hat{q} = q/|q|$ (q is the phonon wave vector) with polarizations α ($\alpha = 1, 2, 3$) is given by

$$v_\alpha(\hat{q}) = \sqrt{C_\alpha(\hat{q})/\rho} \tag{1}$$

where ρ is the mass density. The effective elastic constant $C_\alpha(\hat{q})$ is one of the three eigenvalues of the Christoffel equation

$$C_{ijkl}\hat{q}_j\hat{q}_k u_{l,\alpha} = C_\alpha(\hat{q})u_{l,\alpha} \qquad (i, j, k, l = 1, 2, 3). \tag{2}$$

In (2), the Einstein summation convention is used for repeated indices i, j, k, l. The C_{ijkl} are the components of the elastic stiffness tensor; $u_\alpha = u_{i,\alpha}\hat{x}_i$ is the particle displacement vector

defining the polarization of the sound modes; $\hat{x}_1, \hat{x}_2, \hat{x}_3$ are the unit vectors along three orthogonal directions x_1, x_2, x_3 within the sample, defined according to IRE standards [29]. Using equations (1) and (2) the tensor components C_{ijkl} can be determined by measuring hypersonic velocities $v_\alpha(\hat{q})$ for a sufficient number of pairs (α, q).

An especially suitable way to obtain the desired set of $v_\alpha(\hat{q})$ is the application of the 90A-scattering technique (figure 1(*b*)) [10,23,26,27]. This technique is useful for Brillouin measurements on thin film-like samples of type (ii). Even films of only several micrometres thickness can be studied. In figure 2 is sketched the scattering volume and the method of scanning the sample to obtain a combined space- and angle-resolving BS. For angle-resolving BS the lateral size of the domains within the polydomain film needs hardly to exceed the diameter of the scattering volume (of the order of 100 μm or less). Due to the small thickness of the melt-grown film there is a good chance of growing single-crystalline domains as thick as the melt film. Since crystalline DFTCE is not birefringent the phonon wave vectors q as selected by the 90A scattering geometry are the same for the three acoustic phonon branches and yield the same phonon wavelength $\Lambda^{90A} = 363.8$ nm (vacuum laser wavelength $\lambda = 514.5$ nm) for the quasi-longitudinal (QL) and quasi-transverse (QT) phonons. While turning the sample plate around the 'sample normal' P (figure 1(*b*)), q remains constant relative to the laboratory frame. In the crystal co-ordinate system, q describes a circle of radius $q = (2\pi/363.8)$ nm^{-1} within the plane defined by its normal P. Thus, using the 90A scattering geometry, sound-velocity measurements for many different propagation directions can be performed at a single-crystal domain. Taking advantage of this, the problem of unknown crystallite (domain) orientation can be solved in the following way. First one has to put the scattering volume into a sufficiently large crystal domain. Then, the sound velocities for the selected crystal domain have to be measured by rotating the sample around P for different angles ϕ. Thus according to (2) a set of equations can be written to derive the elastic stiffness constants and three additional parameters specifying the selected plane cut of the related three-sheeted sound-velocity polar diagram. Such measurements can be done even as a function of temperature. An adequate set-up, including temperature control between 4 and 500 K, has been reported recently [10].

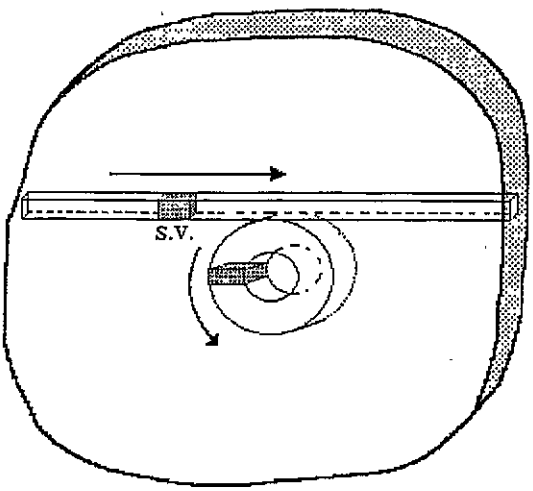

Figure 2. A schematic representation of the scattering volume (SV) and its displacements in a sample due to space- (straight line) and angle-resolving (circle) Brillouin spectroscopy.

In order to obtain insight into the lateral-domain size of thin-film samples of type (ii) we used space-resolving BS (Brillouin scanning microscopy, BSM) [10, 23, 24] on samples crystallized from the melt at different cooling rates. Figure 3 on one hand shows clearly the poly-domain structure of the samples as imaged by the space dependence of the quasi-longitudinal (f_{QL}) and quasi-transverse (f_{QT}) sound frequencies and on the other hand shows that domains with lateral dimensions of several millimetres can be grown on a PIA substrate.

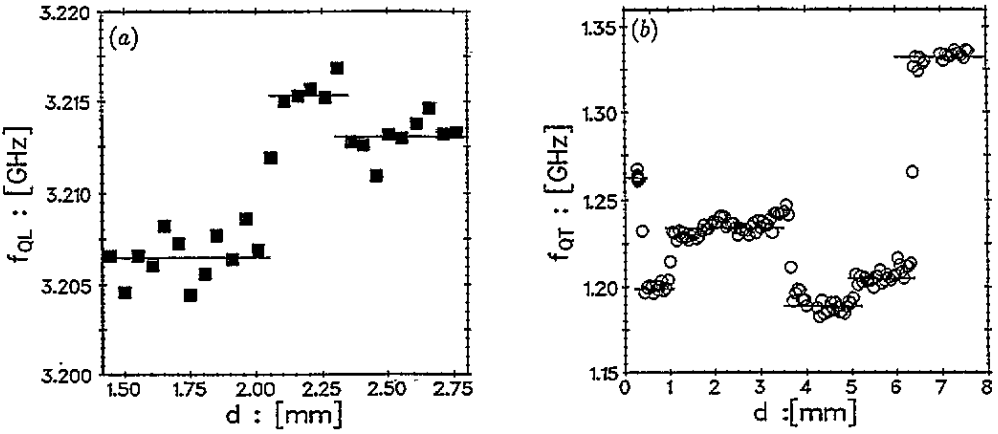

Figure 3. The Brillouin frequency corresponding to (*a*) the quasi-longitudinal mode, f_{QL}, and (*b*) the quasi-transverse mode, f_{QT}, as a function of the position, d, of the scattering volume in a DFTCE sample at $T \simeq 290$ K. The different domains are indicated by guide lines.

2.5. Dielectric spectroscopy

For dielectric measurements, the liquid sample was injected into a small cuvette of 90 mm^3, which formed a coaxial cylindrical capacitor. The cuvette, with a calibrated Pt resistance thermometer (Rosemount 118MF) attached to its flat bottom, was placed into the chamber of a top-loaded cryostat. With He gas as a heat-transmitting medium, this set-up ensured an absolute temperature accuracy of ± 0.5 K. The measurements were carried out during continuous cooling at a rate of (-30) mK s^{-1}.

Three automatic bridges, viz. Tesla BM-595, HP 4274A and HP 4192A, were employed. The frequency range investigated covered 4.5 decades: from 100 Hz to 1.9 MHz. The filled cuvette yielded outside the dispersion region, especially below 2 kHz, very small values of capacitance and loss angle $\tan\delta$. Therefore a standard non-inductive resistor (typically 10–30 MΩ) was connected in parallel to the cuvette outside the cryostat. Such an RC combination yielded measurable values, from which the dielectric data were recalculated. The measuring field amounted to 2 V mm^{-1} (RMS).

3. Results and discussion

Analysing the diffraction pattern, it turns out that the symmetry of DFTCE remains cubic until the lowest measured temperature of about 10 K. The quasi-static glass transition at $T_g = 86$ K is merely accompanied by a slight but detectable increase of the width of the

Bragg peaks. Thus the interpretation of Kishimoto *et al* [9], based on their calorimetric investigation, is supported by this result. The elastic neutron-diffraction measurements were performed at cooling rate of about 0.3 K min^{-1}.

The IR transmission spectra in both the liquid and the solid phase are shown in figure 4. It is seen that the main absorption peaks are present in both phases. The sudden overall drop of the transmission upon solidification is presumably caused by scattering from cracks inside the sample and gaps between the cell windows and the solidified sample.

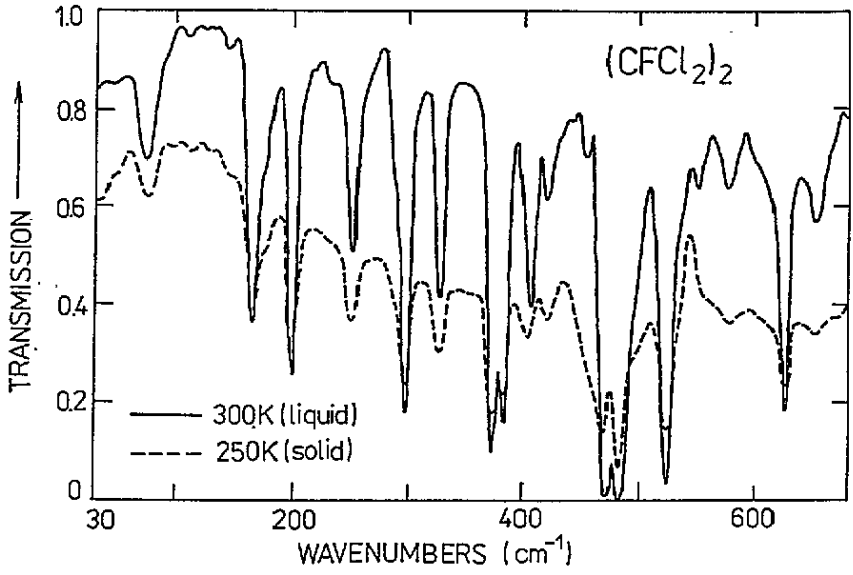

Figure 4. The IR transmission spectrum of DFTCE.

Above 100 cm^{-1} and 250 K no pronounced temperature dependence of the solidified sample transmission was observed. The mode frequencies are 168, 177, 201, 153, 290, 299, 329, 373, 384, 407, 420, 471, 482, 524, 579, 626 and 653 cm^{-1}. Above 270 cm^{-1} these frequencies agree very well with those from the early measurements by Kagarise and Daasch [15].

Below 100 cm^{-1} we observed a mode near 80 cm^{-1}, which we assign to torsion libration of adjacent $CFCl_2$ groups against each other. Our assignment is based on measurements and calculations for an isomorphous molecule ClF_2–ClF_2 [30] where the torsion mode was found even lower (58 cm^{-1}). In our case the torsion mode is present also in the liquid phase (figure 4) and in Raman spectra [30], which excludes its assignment as a homogeneous librational mode. The latter is expected at still lower frequency and actually was only observed in the solid phase as a broad nearly overdamped feature centred near 40 cm^{-1}. This mode plays the role of an attempt frequency for the reorientational molecular motion above the freezing temperature $T_g = 86$ K and compares reasonably well with $\nu_0 = 26$ cm^{-1} from the fit of our dielectric data to the Vogel–Fulcher law (see below).

In figure 5 the temperature dependence of the submillimetre absorption is shown. The most pronounced change concerns the torsion-mode frequency which shifts from ~ 77 cm^{-1} at the melting point to ~ 83 cm^{-1} at 5 K, without measurable anomalies at T_g or temperature dependence of damping (~ 11 cm^{-1}).

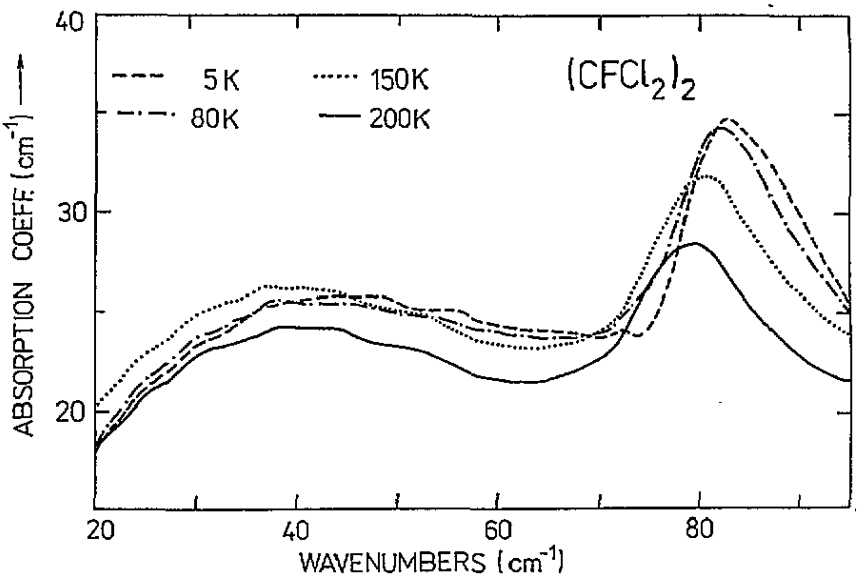

Figure 5. The FIR absorption coefficient α of DFTCE at various temperatures.

It is now firmly established that the molecules structure of DFTCE is a mixture of *trans* and *gauche* isomers. Their concentration ratio above T_g is given by $(N_g/N_t) = 2\exp[-\Delta E/(k_B T)]$, with $\Delta E = 810$ J mol^{-1} [14], so the dipolar *gauche* concentration decreases from $N_g(300\text{ K}) = 0.59$ to $N_g(130\text{ K}) = 0.49$ and then stays constant (frozen) upon further cooling, since the transition time becomes too long in comparison with the experimental time constant. The IR selection rules for molecular vibrations differ for the *trans* and *gauche* form [2]: the *trans* isomer of symmetry C_{2h} has $6a_g + 3b_g + 4a_u + 5b_u$ molecular vibrations (g modes Raman active, u modes IR active) i.e. nine IR modes, whereas the *gauche* isomer of the non-centrosymmetric symmetry C_2 has 10a+8b vibrational modes (both Raman and IR active). The large number of observed IR modes (19 modes below 660 cm^{-1}) and their small temperature dependences agree with the idea that the substance consists of a practically temperature-independent mixture of the two isomers.

Figure 6 shows direct and indirect results of our elastic neutron-diffraction measurements The temperature-dependent specific volume $v_s(T)$ was calculated from lattice constant, a, using $v_s(T) = (a^3(T)/m_u)$, where $m_u = 6.774 \times 10^{-22}$ g is the mass per unit cell of cubic DFTCE. Using the Lorenz–Lorentz equation [31]

$$v_s r = (n^2 + 2)/(n^2 - 1) \tag{3}$$

the temperature-dependent refractive index $n(T)$ was calculated from the specific-volume data v_s after the specific refractivity r had been calibrated by $n_{514.5}(295\text{ K}) = 1.4514$, measured using an Abbé refractometer. The $n(T)$ curve in figure 6 corresponds to the optical wavelength of $\lambda = 514.5$ nm. The temperature-dependent function $v_s(T)$ as well as $n(T)$ shows the characteristic change of the slope at T_g usually observed in canonical fragile glasses. Above T_g both curves show a slight bending versus temperature.

Angle-resolving BS was used to determine the elastic stiffness tensor close to ambient temperature ($T = 290.5$ K). Figure 7 shows frequencies of quasi-longitudinal (f_{QL}) and quasi-transverse acoustic phonons (f_{QT}) as a function of the rotation angle ϕ of the phonon

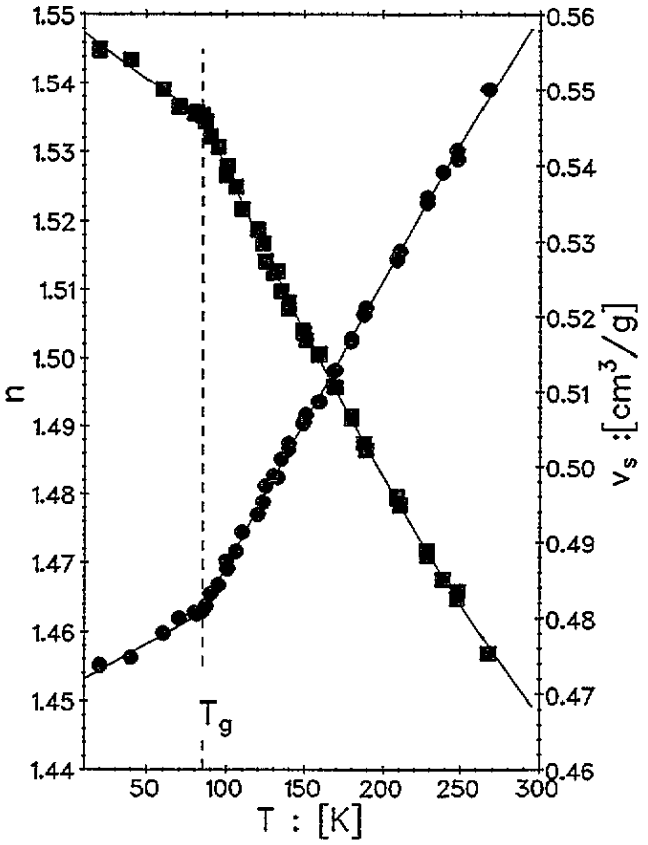

Figure 6. The temperature dependence of the refractive index n (full squares) and specific volume v_s (full circles) of DFTCE. T_g represents the glass-transition temperature $T_g = 86$ K. The lines are only guides to the eye.

wave vector within the plane of the film-like sample. Unfortunately, the scattering cross section of the pure shear mode (elasto-optical coupling) was so small that this mode could not be detected directly. However, following subsection 2.4 we could calculate the complete elastic-stiffness tensor C_{ij} (Voigt notation). Using (2) and the corresponding data (see figure 7) we then calculated appropriate sound-velocity polar diagrams (figure 8) for [100], [110] and [111] symmetry planes. Until now, these time-consuming measurements have been extended down to 228 K. Figure 9 gives the related f_{QL}- and f_{QT}-curves and figure 10 shows the resulting temperature dependence of the stiffness coefficients C_{ij}. It is found that the shear-stiffness coefficient C_{44} shows nearly no temperature dependence although C_{11} increases strongly with decreasing temperature. At 273 K C_{44} is smaller than C_{11} by a factor of six and this factor even increases to a value of seven at about 230 K. A significant anomaly of C_{44} is therefore expected to appear at lower temperatures in the vicinity of T_g (cf [32]).

It is well known that the freezing process strongly reduces the plasticity of glass formers (e.g. [10, 32]). Therefore it is expected that the freezing process strongly influences the elastic properties of the material and that the elastic stiffness coefficients should be a sensitive probe for that. Therefore, we studied the sound velocities of QL acoustic modes as a

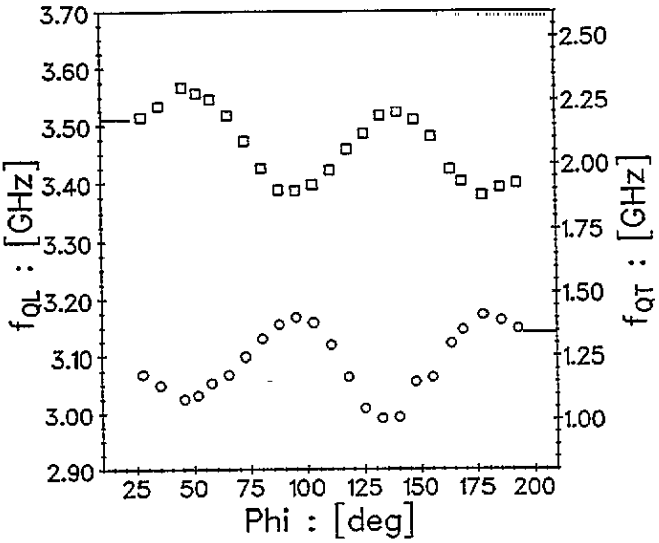

Figure 7. The angular dependence of f_{QL} and f_{QT} close to ambient temperature (see the text).

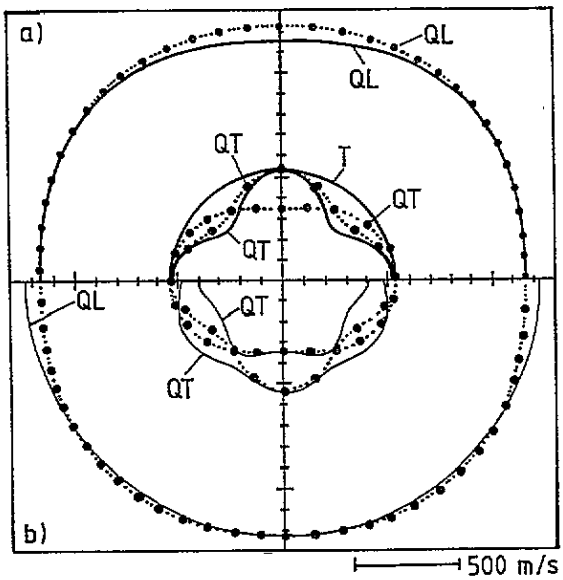

Figure 8. Theoretical polar diagrams of the three acoustic branches (QL, quasi-longitudinal, QT, quasi-transverse and T, pure transverse) calculated using the following values for the three elastic constants involved: $C_{11} = 2.39$ GPa, $C_{12} = 1.96$ GPa, $C_{44} = 0.52$ GPa. The thick line represents the polar diagram on a [100] symmetry plane, the full circles that on a [110] symmetry plane and the thin line that on a [111] symmetry plane.

function of temperature as well as a function of wave vector using the 90A and the 90N scattering geometries. These results are presented in figures 11–13. As might be estimated from figure 8 every QL mode has nearly longitudinal polarization, therefore, to a good approximation all measurements given in figures 11–13 reflect the temperature behaviour

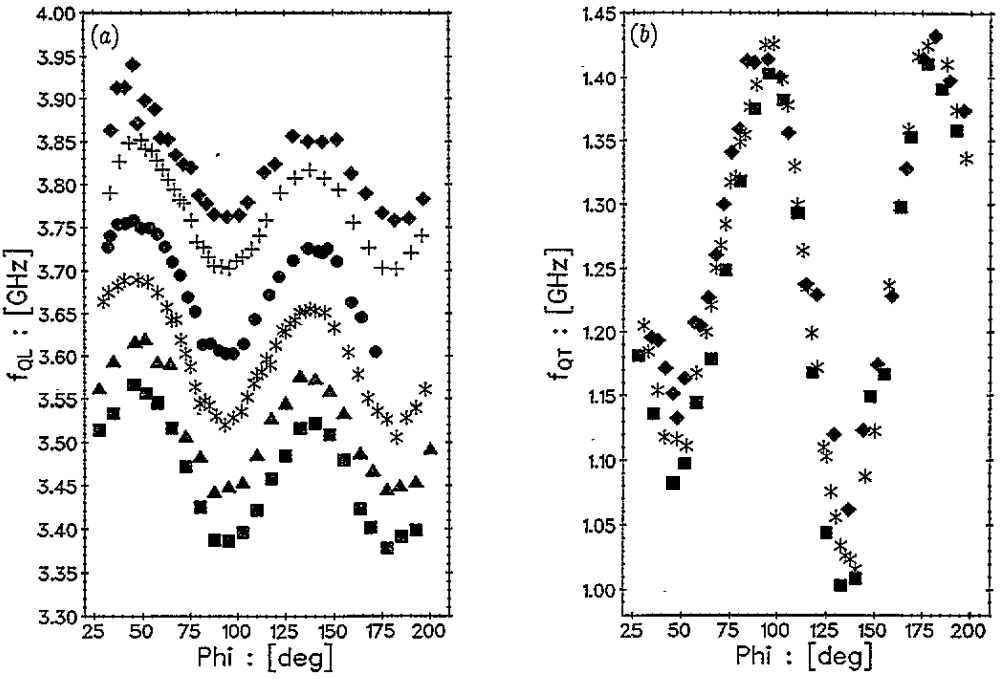

Figure 9. (*a*) The temperature evolution of the angular dependence of the quasi-longitudinal branch on a plane with random orientation in space: squares, $T = 272.9$ K; triangles, $T = 267.8$ K; stars, $T = 258$ K; full circles, $T = 248$ K; crosses, $T = 238.1$ K; diamonds, $T = 229.2$ K. (*b*) The same as in (*a*) but now for the quasi-transverse branch. For the sake of clarity only three temperatures are presented. Squares, $T = 272.9$ K; stars, $T = 258$ K; diamonds, $T = 228.2$ K.

of the pure longitudinally polarized sound mode, i.e. $v(T) \cong v_L(T) = \sqrt{C_{11}(T)/\rho(T)}$. At first sight $v(T)$ behaves similarly to what is found at hypersonic frequencies for fragile glasses like atactic (amorphous) polymers (cf [10]). In accordance with the temperature behaviour of the specific volume (figure 6) the slope of the sound velocity curve $v(T)$ changes characteristically at T_g (kink-like behaviour). At higher temperatures, above the quasi-static glass transition at $T_g = 86$ K, there exists a steel increase of the sound velocity, but a striking concave bending in the $v(T)$-curve can be seen at $T^* \simeq T_g + 60$–70 K. On one hand such a temperature dependence does not correspond to the transition from the 'fast-motion' to the 'slow-motion' regime of an appropriate structural relaxation process (cf [10]). On the other hand, within the margin of error (uncertainty of the wave vector orientations for the different measurements) there is no wave vector dependence either of sound velocity or of sound attenuation (figure 13). although the acoustic wavelength was changed by a factor of ~ 1.6 turning from the 90A to the 90N scattering geometry. This is not the expected behaviour of the classical structural glass relaxation (α-process). Therefore, the mechanism leading to the observed $v(T)$-curve should be at least of local origin (further discussion of this is presented below).

Figure 14 shows typical permittivity behaviour of solid DFTCE in the range of dielectric relaxation. With increasing frequency f, the maxima of $\varepsilon(T)$ and $\tan\delta(T)$ shift towards higher temperatures. At temperatures well above and below these maxima, the dielectric dispersion is practically not measurable within the frequency region investigated. In

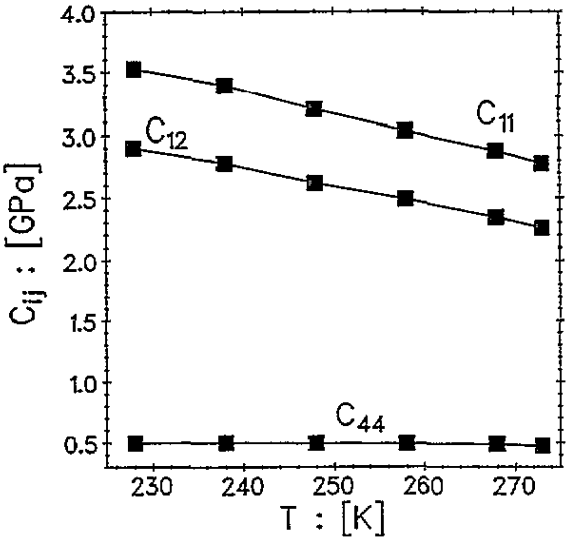

Figure 10. The temperature dependence of the components of the elastic-stiffness tensor (cubic symmetry) as obtained from the least-squares fits of the polar diagrams shown in figure 9.

an additional experiment with a plane-parallel capacitor (cuvette) we determined the permittivity value of DFTCE at the ice point to be $\varepsilon_{273K} = 3.040 \pm 0.006$, for frequencies between 1 and 20 kHz. This value has to be compared with the dielectric constant measured at optical frequencies $\varepsilon_{268K}(\lambda = 514.5 \text{ nm}) = 2.12$ indicating the existence of a small dispersion. Though we use and present only data taken on cooling in this study, we measured the entire cooling–heating cycle to check for the formation of cracks inside the sample. Measurements that exhibited sudden discontinuities in the permittivity value were discarded. During these cycles we found no manifestation of the presence of an ordered phase, which forms only after very long low-temperature annealing [9]. No temperature hysteresis was observed in the positions of the ε and $\tan\delta$ maxima in these cycles. These positions also remain unaffected by an applied DC field up to 10 MV m^{-1}.

The observed dielectric dispersion is a manifestation of the primary relaxation associated with the glass transition. It is a standard procedure to use the positions of the $\tan\delta$ maxima on the temperature scale (data for 25 frequencies in our case) for analysis by the Arrhenius and/or Vogel–Fulcher law. The Arrhenius fit, however, yielded an unreasonably high attempt frequency $\omega_0 \cong 7.4 \times 10^{32}$ s^{-1}, not a rare situation in the case of glass transitions (see e.g. [33]). Figure 15 shows the fit to the Vogel–Fulcher law ($\omega_{max}(T) = \omega_0 \exp(-E/(T - T_{VF}))$, in which only data from our dielectric measurements were employed. The best values of the least-squares fit (at $r^2 = 0.9988$; r is the correlation coefficient) are $\omega_0 = 8.44 \times 10^{11}$ Hz ($\nu_0 = 28.1$ cm^{-1}), the activation energy $E = 0.048$ eV and the Vogel–Fulcher temperature $T_{VF} = 70.42$ K. On this graph, the frequency of the attenuation maximum of a QL acoustic phonon with $f_{QL}^{90A} = 4.35$ GHz occurring at 160 K was added, together with data taken from figure 11 of [34] (which shows the temperature dependence of the correlation time τ_r of the molecular reorientation in DFTCE, as determined from NMR experiments). The mutual agreement of all these data is good. The rather high discrepancy between NMR and dielectric data at the lowest temperature in figure 15, which is very close to T_g, possibly gives a hint that the Vogel–Fulcher law is not valid down to the glass-transition temperature, as is often observed. Considering only the temperature dependence of the relaxation time of

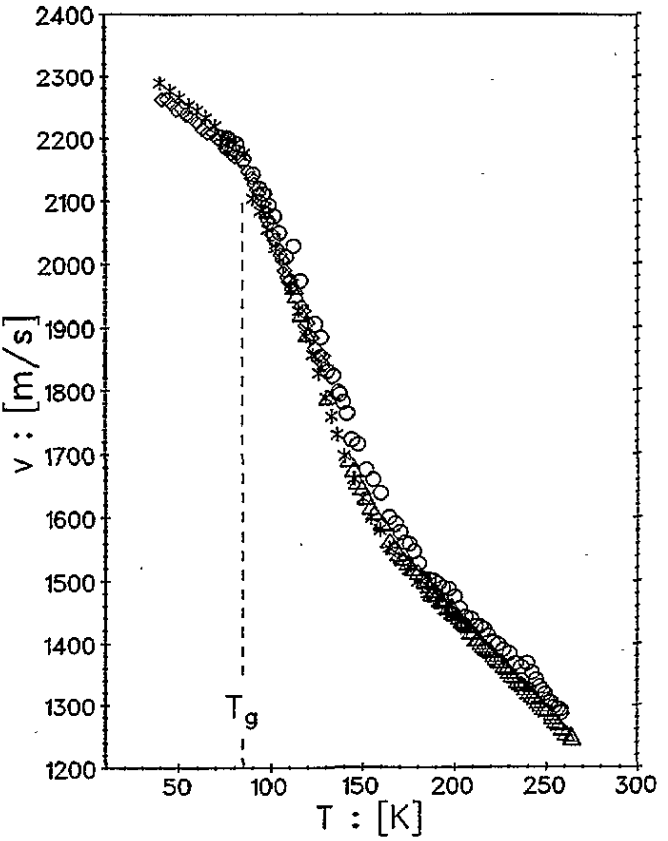

Figure 11. The temperature dependence of the sound velocity $v(T)$ as obtained from the 90A measurements on a PIA substrate. At the glass-transition temperature ($T_g = 86$ K) one observes a bending anomaly typical of canonical glasses. Different symbols denote different cooling and heating runs.

different relaxation processes it could be concluded that the relaxation process observed in the dielectric measurements is a manifestation of freezing out of the reorientation of DFTCE molecules. This fit also yields a reasonable 'frequency of non-ergodicity', i.e. the frequency at the thermodynamic glass-transition temperature $T_g = 86$ K: it is 0.46 Hz.

Over a wide temperature region below ambient temperature, crystalline DFTCE shows interesting freezing phenomena. The structural elements and the dynamical and quasi-static disorder of this system are reminiscent of the so-called orientational glasses such as KCN–KBr (see [35]). However, at least two characteristic differences are observed. Firstly a dramatic jump in the heat capacity and, consequently, typical kink-like anomalies in the specific volume and in the sound velocity were found at the quasi-static glass-transition temperature T_g. So far such anomalies are not known for orientational glasses. Secondly relatively far away from the transition point T_g ($T \simeq T_g + 50$–70 K) the dynamics of freezing is peculiar and more similar to the behaviour of structural relaxation in classical fragile glasses. Therefore in earlier works the freezing in DFTCE was discussed in terms of the classical idea of co-operative α- and β-processes.

However, looking at the temperature dependence of the frequencies of acoustic phonons,

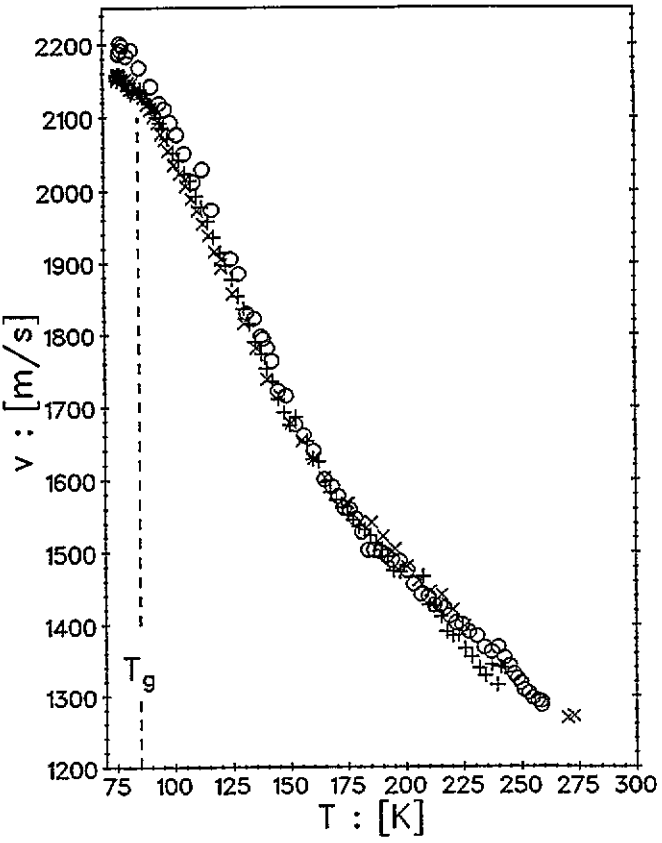

Figure 12. A comparison of $v(T)$ as obtained from 90A (○, PIA substrate) and 90N measurements (+, ×, cylindrical sample)($T_g = 86$ K).

measured by BS (see above and [18]), some doubts arise concerning this 'classical' interpretation. A continuous freezing of the molecular reorientations would produce a smooth change of the phonon frequencies on lowering the temperature. At best an S-like behaviour could be observed at temperatures where $\omega\tau(T) \simeq 1$. Actually a relatively sharp change in the slope of the temperature-dependent acoustic-phonon frequency was found at about 170 K, where at the same time the attenuation of this acoustic-phonon mode shows a maximum (see figure 13). In contrast to this, the attenuation-peak position for a classical relaxation process would coincide with the turning point of the curve $f_{QL}(T)$, where the curvature is zero. Moreover, the attenuation damping peaks measured in the 90A ($f_{QL}^{90A} \simeq 4$ GHz) and 90N scattering geometries ($f_{QL}^{90N} \simeq 7$ GHz) yield damping peaks at nearly the same temperature. That means that the characteristic attenuation-peak shift expected on the basis of the Vogel–Fulcher law is not really confirmed by the Brillouin data (a shift of the order of 20 K should occur).

Therefore alternative explanations of the relaxation processes in DFTCE have to be searched for. Several attempts to incorporate collective relaxational effects in describing non-Debye relaxation have been made (see e.g. [2, 4, 36]). However, it is of interest to discuss our results in the light of a recent mode-coupling theory for the scalar φ^4-lattice model of structurally unstable systems [20]. On the basis of this theory a dynamic freezing

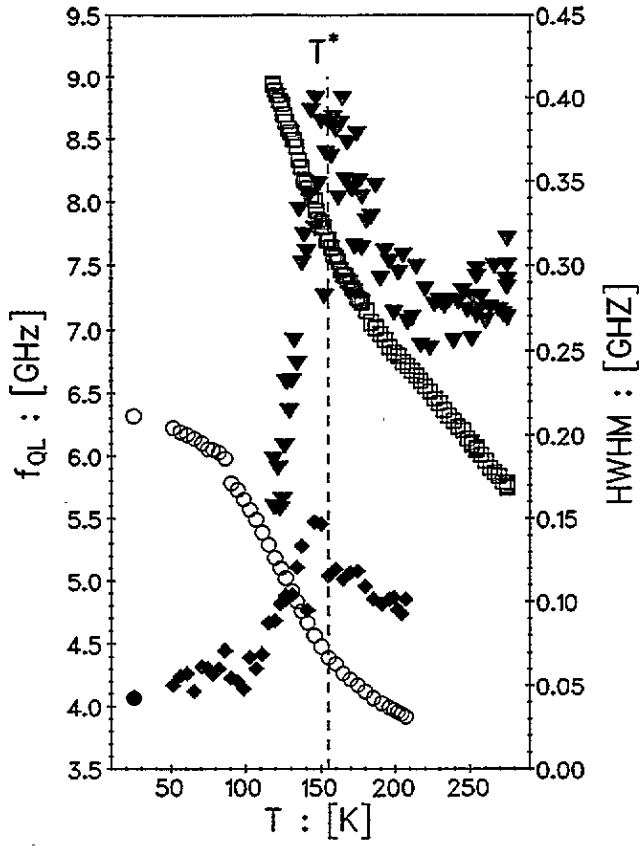

Figure 13. A comparison between $f_{QL}(T)$ and the corresponding hypersonic attenuation (HWHM) using the 90A (O, ♦) and 90N (□, ▼)scattering geometries. The dashed line reflects a characteristic temperature T^*, which may be interpreted as the mode-coupling freezing-transition temperature T_s^*.

transition is obtained at a temperature T_c^* well above the static structural phase transition temperature T_c†. Using the results of this theory the following scenario is conceivable (cf [20,21]). At higher temperatures ($T > 200$ K) the main relaxation process is connected with jumps of individual DFTCE molecules between the four different orientations along the (111)-direction. This relaxation was observed around the melting point by Satija and Wang [14] when analysing the Rayleigh line width of the Brillouin spectra. At least in this temperature range the relaxation data fit the Arrhenius law quite well with the following reasonable parameters: activation energy $E_a = 0.087$ meV and attempt frequency $\omega_0 = 136.9$ cm^{-1}. Lowering the temperature, data of neutron scattering [37], and of Raman [38] and our FIR spectroscopy, point to a new kind of dynamics in the frequency region 20–50 cm^{-1}, which can be assigned to a homogeneous librational mode. Taking into account the anharmonicity of the local potential for the rotation of DFTCE dumbbells and a random distribution of *trans* and *gauche* states of the DTFCE molecules it seems possible to

† The mode-coupling treatment in [20] is formally similar to that of the dynamical theory of glass transitions in supercooled liquids developed by Götze and Sjögren [5]. It is not clear to us whether the freezing of librational motion can be compared with the freezing of density–density fluctuations leading to the transition of fragile glasses.

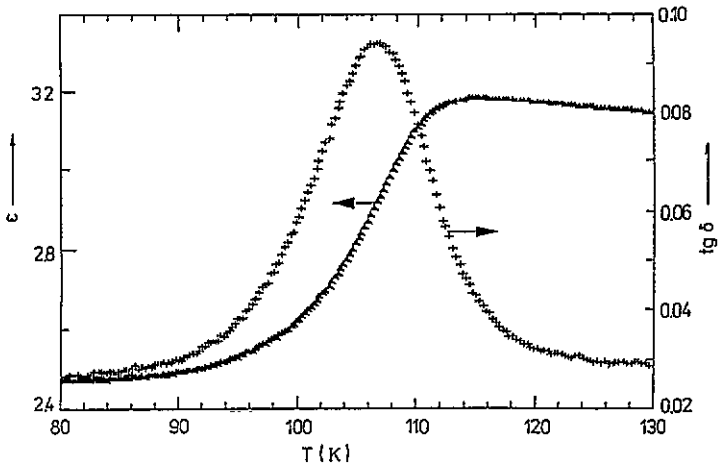

Figure 14. The temperature dependence of the permittivity ε and losses ($\tan\delta$) of DFTCE at 200 kHz, taken on cooling.

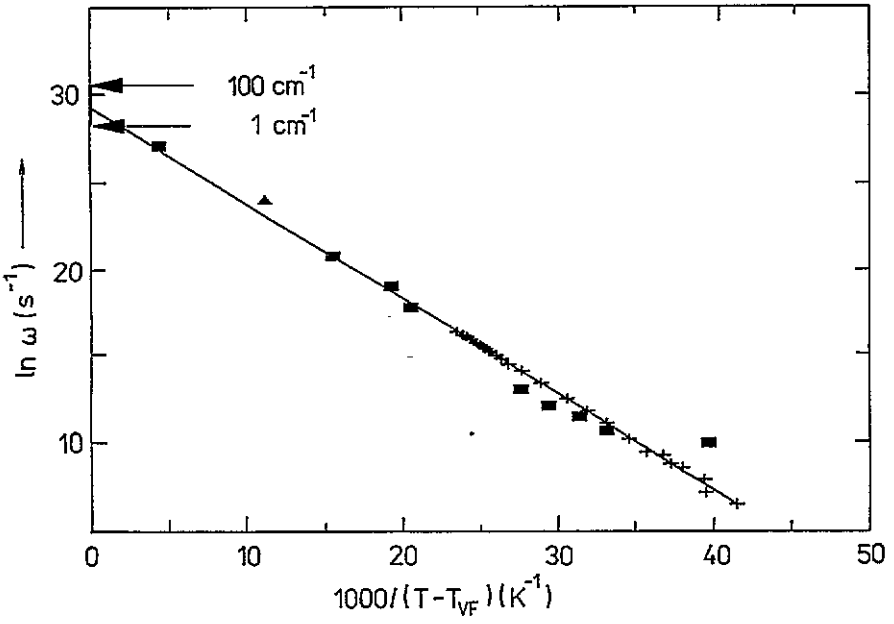

Figure 15. The Vogel–Fulcher plot for DFTCE: +, the temperature dependence of the $\tan\delta$ maximum at different frequencies; solid line, least-squares fit (T_{VF} = 70.432 K, ω_0 = 8.4410^{11} Hz and E = 0.048 eV); ▲, Brillouin value; ■, correlation frequencies of molecular reorientations in DFTCE (taken from [39]).

describe this librational dynamics with the model presented in [20]. The results of the mode-coupling theory obtained in [20] can then be used for qualitative discussions. According to these a freezing transition in the librational subsystem at a temperature T_g^* above the static glass-transition temperature T_g is expected. Owing to the disorder of a so-called A-type

transition (cf [5]) is expected where the imaginary part of the dynamical order-parameter susceptibility shows a pronounced peak around the temperature T_g^*, while the real part of that susceptibility has a cusp there. Because of the absence of the local inversion symmetry in DFTCE the interaction of the librational motion with the acoustic phonons can be caused by a coupling term linear in the order parameter. This circumstance may produce a phonon attenuation peak and the change in slope of the temperature-dependent phonon frequency at $T^* = 170$ K. According to the mode-coupling theory at $T < T^*$ a central peak component in the fluctuation spectrum appears, but its intensity vanishes as T goes to T^*. Owing to remaining thermally activated processes this central peak will have a finite width corresponding to the relaxation of correlated clusters of DFTCE molecules. This is the relaxation process seen by our dielectric and NMR [39] measurements. To check this idea it would be necessary to observe the intensity of the dielectric loss peak up to temperatures $T \simeq T^*$, where this peak should disappear. So far we have not been able to perform such measurements since our dielectric equipment works only to megahertz frequencies, while gigahertz are required. A detailed discussion of the proposed interpretation will be given elsewhere [19].

4. Conclusions

Solid difluorotetrachloroethane exhibits freezing phenomena that partly resemble orientational glasses and partly canonical glasses. Within the accuracy of experimental results the overall relaxation frequency seems to obey the Vogel–Fulcher temperature dependence, but analysing the Brillouin-scattering data it seems likely that the temperature dependence of the sound frequencies and of the corresponding attenuation reflects a new kind of freezing process, which may be caused by anomalies in the librational motion. One possible explanation of this behaviour was discussed in the framework of a mode-coupling theory [20] applied to the orientation dynamics of the DFTCE molecules. According to this approach the high-frequency relaxation above the freezing temperature $T_g^* \cong 170$ K is due to reorientation of individual molecules, whereas the low-temperature relaxation below T_g^* should be due to correlated motion of locally ordered molecular clusters. Combined Raman and Brillouin-scattering measurements over several frequency decades (cf [40]) and dielectric spectroscopy in the gigahertz range are needed to confirm the mode-coupling predictions of a dynamical freezing transition in DFTCE.

Acknowledgments

This work was partly supported by the Deutsche Forschungsgemeinschaft. We acknowledge very fruitful discussions with Professor H-G Unruh and Dipl. Phys. J Schweigert. We are grateful to Dr H Hammer for helpful discussion, and purification and chemical characterization of DFTCE material. The dielectric and FIR spectroscopy measurements were supported by grant No 11081 of the Academy of Sciences of the Czech Republic.

References

[1] Wong J and Angell C A 1976 *Glass Structure by Spectroscopy* (New York: Dekker)
[2] Jäckle J 1986 *Rep. Prog. Phys.* **49** 171

[3] Richter D, Dianoux A J, Petry W and Teixeira J (ed) 1989 *Dynamics of Disordered Materials* (Berlin: Springer)
[4] Elliott S R 1990 *Physics of Amorphous Materials* (New York: Longman Wiley)
[5] Götze W and Sjögren L 1992 *Rep. Prog. Phys.* **55** 241
[6] Descamps M and Caucheteux C 1987 *J. Phys. C: Solid State Phys.* **20** 5073
[7] Hohlwein D, Nägele W and Prandl W 1979 *Acta Crystallogr.* B **35** 2975
[8] Gerlach P 1984 *PhD Thesis* University of Tübingen
[9] Kishimoto K, Suga H and Seki S 1978 *Bull. Chem. Soc. Japan* **51** 1691
[10] Krüger J K 1989 *Optical Techniques to Characterize Polymer Systems* ed H Bässler (Amsterdam: Elsevier)
[11] Locke E G, Brode W R and Henne A L 1934 *J. Am. Chem. Soc.* **56** 1726
[12] Vogel L 1980 *Wiss. Z. Univ. Halle, Math.-Naturw. Reihe* **29** 5
[13] Iwasaki M, Nagase S and Kojima R 1957 *Bull. Chem. Soc. Japan* **30** 230
[14] Satija S K and Wang C H 1978 *J. Chem. Phys.* **69** 1101
[15] Kagarise R E and Daasch L W 1955 *J. Chem. Phys.* **23** 113
[16] Pethrick R A and Wyn-Jones E 1971 *J. Chem. Soc.* A 54
[17] Newmark R A and Senderholm C H 1965 *J. Chem. Phys.* **43** 602
[18] Wang C H and Satija S K 1982 *Chem. Phys. Lett.* **87** 330
[19] Schreiber J, Krüger J K, Jiménez R, Unruh H-G and Legrand J F to be published
[20] Aksenov V K, Kornilov E I and Schreiber J 1993 *J. Phys.: Condens. Matter* **23** 5067
[21] Schreiber J, Krüger J K, Jiménez R and Legrand J F 1991 *Proc. 2nd Meeting on Disorder in Molecular Solids (II) (Garchy, 1991)* ed M Deschamps (Villeneuve d'Ascq: UFR de Physique)
[22] The material was kindly supplied by Dr H Hammer, RWE Gesellschaft für Forschung und Entwicklung, Köln, Germany
[23] Krüger J K, Jiménez R, Bohn K-P, Petersson J, Albers J, Klöpperpieper A, Sauerland E and Müser H-E 1990 *Phys. Rev.* B **42** 8537
[24] Krüger J K, Prechtl M, Wittmann J C, Meyer S, Legrand J F and D'Asseza G 1993 *J. Pol. Sci.* B **31** 505
[25] Krüger J K, Prechtl M, Smith P, Meyer S and Wittmann J C 1992 *J. Polym. Sci.* B **30** 1173
[26] Krüger J K, Peetz L and Pietralla M 1978 *Polymer* **19** 1397
[27] Krüger J K, Marx A, Peetz L and Unruh H-G 1986 *Colloid Polym. Sci.* **264** 403
[28] Marx A, Krüger J K and Unruh H-G 1988 *Appl. Phys.* A **47** 367
[29] 1949 *IRE Proc. Standards on Piezoelectric Crystals* **37** 1378
[30] Powell D L, Gustavsen J E, Klaeboe P and Nielsen C J 1978 *J. Raman Spectrosc.* **7** 111
[31] Böttcher C J F 1973 *Theory of Electric Polarization* vol I (Amsterdam: Elsevier)
[32] Jiménez R, Bohn K-P, Krüger J K and Petersson J 1990 *Ferroelectrics* **106** 175
[33] Böhmer R and Loidl A 1990 *Phys. Rev.* B **42** 1439
[34] Stokes H T, Case T A, Ailion D C and Wang C H 1979 *J. Chem. Phys.* **70** 3563
[35] Michel K H 1987 *Z. Phys.* B **68** 259
[36] Jonscher A K 1983 *Dielectric Relaxation in Solids* (London: Chelsea Dielectrics)
[37] Jiménez R 1993 *PhD Thesis* University of Saarland
[38] Schweigert J 1991 *Diploma-thesis* University of Saarland
[39] Stokes H T, Case T A, Ailion D C and Wang C H 1979 *J. Chem. Phys.* **70** 3563
[40] Li G, Du W M, Chen X K and Cummins H Z 1992 *Phys. Rev.* A **45** 3867